applied optics

Signal correction by detection of scanning position in a white-light interferometer for exact surface profile measurement

Songjie Luo,[1] Takamasa Suzuki,[1,*] Osami Sasaki,[1,2] Samuel Choi,[1] Ziyang Chen,[2] and Jixiong Pu[2]

[1]Graduate School of Science and Technology, Niigata University, Niigata 950-2181, Japan
[2]Fujian Provincial Key Laboratory of Light Propagation and Transformation, College of Information Science and Engineering, Huaqiao University, Xiamen, Fujian 361021, China
*Corresponding author: takamasa@eng.niigata-u.ac.jp

Received 30 January 2019; revised 7 April 2019; accepted 7 April 2019; posted 8 April 2019 (Doc. ID 358951); published 29 April 2019

In order to perform an exact surface profile measurement with a white-light scanning interferometer (WLSI), an actual optical path difference (OPD) changing with time is detected with an additional interferometer in which the light source of the WLSI and an optical band-pass filter are used. This interferometer is simply equipped in the WLSI and does not negatively influence the WLSI. The real OPD is easily calculated from an interference signal with the same signal processing as that in the WLSI. The interference signal of the WLSI is corrected with the real OPD values or the real scanning position values. The corrected interference signal with a constant sampling interval is obtained with an interpolation method. With this correction method, a surface profile with a step shape of 3-μm height is measured accurately with an error less than 2 nm.

https://doi.org/10.1364/AO.58.003548

1. INTRODUCTION

White-light scanning interferometers (WLSIs) have been widely used for measurement of a reflecting surface profile with a step shape whose height is more than a few micrometers. Since this measurement is very important to develop electronic devices with surface profiles of nano-order structures, advanced signal processing is required to make exact measurements with nanometer order accuracy. When a WLSI satisfies two conditions—(1) all of the wavenumbers have the same optical path difference (OPD) and (2) the OPD changes linearly with time—the interference signal of a WLSI becomes an ideal one whose envelope peak exists at the object position and whose waveform is symmetric about the object position along the scanning positions. In this situation, exact surface profile measurements can be easily achieved. However, in practical situations, these conditions are not satisfied.

First, when the propagation distances of the object and the reference waves in a dispersive medium are not equal, the condition of (1) is not satisfied. Then the waveform of the interference signal becomes non-symmetric for the object position. In this case, the object position is considered to be a scanning position, where the phase of the interference signal is zero nearest the position of the envelope peak. This object position was calculated by the phase-shifting method [1] and the lock-in evaluation method [2]. These two methods focus on the waveform of the real-valued interference signal itself. On the other hand, Fourier transform of the real-valued interference signal or the spectral distribution in wavenumber domain contains useful information about the interference signal. The object position was obtained from the slope in the spectral phase distribution at a central wavenumber [3,4]. The relationships between the spectral phase distribution and the waveform of the real-valued interference signal were analyzed in detail to obtain the position of zero phase nearest the position of envelope peak from the spectral phase distribution [5]. This position of zero phase can be easily obtained from the complex-valued interference signal (CVIS) of the WLSI calculated through inverse Fourier transform of the spectral distribution [6]. Moreover by replacing the phase distribution with a linear phase distribution calculated with least square method, the position of zero phase in this CVIS provides a more accurate object position without suffering from the dispersion effect [7].

Next, when the scanning speed of the reference surface generated by a piezoelectric transducer (PZT) is not constant and the optical components in the WLSI are vibrated by external disturbances, the OPD of the WLSI does not change linearly with time. In order to satisfy the condition of (2), correction methods by using the interference signal detected in WLSI were proposed [8–10]. In Ref. [8], an inclined optical flat surface is measured before and after an exact step displacement is given to the flat surface. Since the step displacement is controlled exactly by an additional interferometer, the scanning position error can be obtained from the two measured surface profiles. This calibration measurement must be made prior to the surface profile measurement. Thus it is desirable to calculate the scanning

positions from the interference signal detected in the surface profile measurement. The spectral distribution of the detected interference signal was analyzed to get the scanning positions [9]. The scanning positions were calculated by applying the phase-shifting interferometry to the detected interference signal [10]. However, when the interference signal contains a dispersion phase, the above two methods cannot extract the exact scanning positions. For this reason, a monochromatic laser interferometer equipped in the WLSI is required to detect the time-varying OPD or the scanning position of the WLSI. There are two important issues regarding the monochromatic laser interferometer: one is that the laser interferometer does not negatively influence the WLSI, and the other is that the signal processing to extract the phase from the interference signal is simple. The configuration of the monochromatic laser interferometer and the signal processing were reported [11]. Algorithms were proposed to calculate the object position while incorporating the detected scanning positions into the calculation [12]. Actual experimental setups were constructed [13,14]. In Ref. [13], two beam splitters for the laser interferometer produce a dispersion effect in the WLSI, and the two interference signals with a known phase difference have to be detected at the same time to extract the interference phase. In Ref. [14], a mirror vibrated by a sinusoidal waveform is used as a reference surface to extract the phase of the laser interferometer, but the signal processing becomes complicated due to the sinusoidal phase modulation, and this phase modulation appears in the interference signal of the WLSI.

In this paper, the two interfering beams in the WSI can be utilized to detect the time-varying OPD, since a supercontinuum light source for the WLSI has strong power. A beam splitter is put in front of a camera for the WLSI in order to divide the two beams of the WLSI for the laser interferometer, and an optical band-pass filter is put in front of a photodiode to detect the signal of the laser interferometer. The time-varying OPD or the scanning positions can be easily and exactly obtained from this interference signal through the same signal processing as that of the WLSI. The calculated scanning positions are assigned to the corresponding sampling points of the interference signal detected in the WLSI. Since the sampling interval in the interference signal corrected with the calculated scanning positions is not constant, the interference signal with a constant sampling interval is interpolated from the interference signal detected in the WLSI. This correction method for the scanning position leads to the excellent result in which the condition of (2) is satisfied through eliminating the non-constant movement of the PZT completely and the effect of random noise caused by external disturbances. These characteristics are made clear by simulations. In experiments, a surface profile with a step shape of 3-μm height is measured accurately with an error less than 2 nm.

2. PRINCIPLE

Figure 1 shows a WLSI with a supercontinuum light source whose spectral intensity is $I(\sigma)$, where σ is the wavenumber. A beam collimated with lens L1 is divided into two beams by a beam splitter (BS1). The position of an object surface is denoted by z_o, and the position of a reference surface is denoted by $z_R(t)$ which is changed by a PZT with time t. Two lenses of L2 and L3 make the optical fields on the object surface

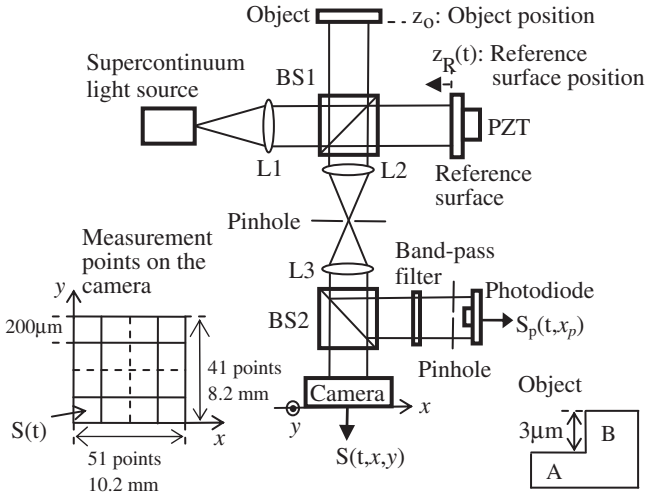

Fig. 1. Schematic of a white-light scanning interferometer.

and the reference surface on a camera. Although the measurement points of the camera are on an x-y plane, equations are described only on the x axis for the sake of simplicity. Denoting the scanning position by $z(t)$, an interference signal detected on the measurement point of the camera is expressed as

$$S(t,x)=\int_{-\infty}^{\infty} I(\sigma)\cos\{4\pi[z(t)-z_o(x)]\sigma+\varphi_d(\sigma,x)\}\mathrm{d}\sigma+n_A(t), \tag{1}$$

where the scanning position is given by

$$z(t)=z_R(t)+z_n(t)=V_a t+z_v(t)+z_n(t). \tag{2}$$

The scanning position contains the two following components: one is the reference surface position $z_R(t)$, which consists of a constant speed V_a and non-linear movement $z_v(t)$ of the PZT, and the other one is a random change $z_n(t)$ generated by external disturbances in the interferometer. The $n_A(t)$ is additive noise. The phase $\varphi_d(\sigma,x)$ is dispersion phase generated by BS1. Since the lengths of the two sides in the BS1 are different, the two beams reflected from the object surface and the reference surface have different path distances of l_1 and l_2 in BS1, respectively, as shown in Fig. 2. Denoting the distance difference by $l_\varepsilon=l_2-l_1$, the dispersion phase is given by

$$\varphi_d(\sigma,x)=4\pi n(\sigma)l_\varepsilon(x)\sigma, \tag{3}$$

where $n(\sigma)$ is the refractive index of the beam splitter, and $l_\varepsilon(x)$ is a linear function of the position x where the two beams go

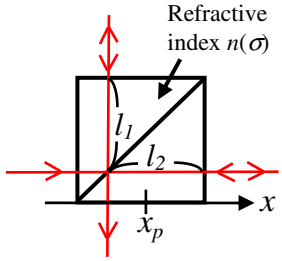

Fig. 2. Generation of dispersion phase by the distance difference of $l_\varepsilon=l_2-l_1$ in BS1.

out from the beam splitter. The beams at the position x_p go to a photodiode.

The beams are divided by BS2 in front of the camera, and the reflected beams are passed through a band-pass filter with the transmission wavenumber σ_f. The photodiode receives the beams coming from the position of $x = x_p$ on BS1 with a pinhole, as shown in Figs. 1 and 2. An interference signal detected with the photodiode is expressed as

$$S_p(t, x_p) = I(\sigma_f)\cos\{4\pi[z(t) - z_o(x_p)]\sigma_f + \varphi_d(\sigma_f)\}. \quad (4)$$

The additive noise in $S_p(t, x_p)$ is ignored because the additive noise generated in the photodiode is very week compared to the $n_A(t)$ generated in the camera and causes a very small error in calculated position value. In order to get a wrapped phase distribution of $S_p(t, x_p)$, inverse Fourier transform is performed on the distribution in the positive frequency region of the Fourier transform of $S_p(t, x_p)$. After obtaining an unwrapped phase of $S_p(t, x_p)$, the phase is divided by $4\pi\sigma_f$ to obtain position value $z_c(t)$, which is given by

$$z_c(t) = z(t) - z_o(x_p) + z_b, \quad (5)$$

where $z_b = n(\sigma_f)l\varepsilon(x_p)$ with Eq. (3). This scanning position value enables the conversion of the time in the signal $S(t)$ to the scanning position $z_c(t)$. Thus, a corrected interference signal is obtained as

$$S(z_c, x) = \int_{-\infty}^{\infty} I(\sigma)\cos[4\pi(z_c - z_o(x) + z_o(x_p) - z_b)\sigma + \varphi_d(\sigma)]\mathrm{d}\sigma + n_{AC}(z_c), \quad (6)$$

where the $n_{AC}(z_c)$ is the additive noise converted from $n_A(t)$. The effects of non-constant movement of the PZT and the random phase changes are eliminated in the corrected signal $S(z_c, x)$. If the dispersion phase $\varphi_d(\sigma)$ is equal to zero, the peak position of the interference signal appears at $z_c = z_o(x) - z_o(x_p) + z_b$. There is a constant shift of the peak position of $-z_o(x_p) + z_b$, which produces parallel displacement in a measured surface. But this displacement does not have any influence on surface profile measurement, because the measured position of a surface is a relative value in an interferometer. Hereafter, the constant shift is ignored.

Figure 3 shows how the corrected signal $S(z_c)$ is obtained from the detected signal $S(t)$. The blue curve is the position value of $z_c(t) = z(t) - z_o(x_p) + z_b$ obtained from the interference signal $S_p(t)$. The small circle denotes the sampling time, and the value of $z_c(t)$ corresponding to the sampling time is indicated with a small triangle. The value of the signal $S(t)$ detected at the sampling time is indicated with a small square. This sampled value of $S(t)$ corresponds to the position value $z_c(t)$, which becomes the value of the horizontal axis in the corrected signal $S(z_c)$. Thus, this correspondence makes the corrected signal $S(z_c)$. Since the interval between the adjacent sampling points of the interference signal $S(z_c)$ is not constant, interpolation is carried out to get the interference signal whose sampling interval is constant.

This corrected interference signal with a constant sampling interval is processed to get the object position z_o with the signal processing reported in Ref. [7]. The amplitude and phase distribution in wavenumber domain or the spectral distribution is

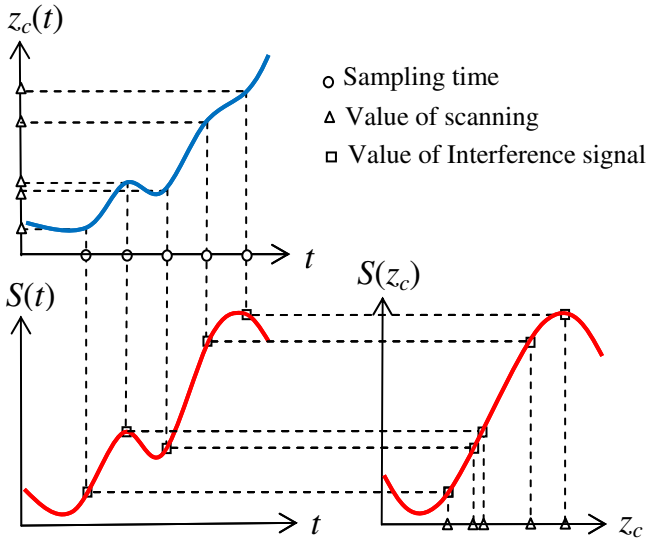

Fig. 3. Correction of the detected signal $S(t)$ by detection of the position value $z_c(t)$.

obtained from Fourier transform of $S(z_c)$. A linear fitted line in the phase distribution is calculated by least square method. Inverse Fourier transform is performed on the spectral distribution whose phase distribution is replaced with the linear fitted line to get the CVIS. A position of maximum amplitude in the CVIS is denoted as z_a. The position z_p of zero phase nearest the position z_a in the CVIS is the measurement value of z_o. The measurement value z_p in the corrected signal $S(z_c)$ is expected to provide high measurement accuracy, which is verified by simulations and experiments in the following sections.

3. DETECTION OF THE SCANNING POSITION AND ITS COMPONENTS

The process to obtain the real scanning position value $z_c(t)$ from $S_p(t, x_p)$ is explained in detail. In order to prevent the leakage effect in Fourier transform, a Gaussian window was used for $S_p(t, x_p)$. Fourier transform was performed on the windowed $S_p(t, x_p)$ whose data number N and interval of Δt were 128 and 0.5 ms, respectively. The wrapped phase of $S_p(t, x_p)$ was obtained by performing inverse Fourier transform on the positive frequency components of the Fourier transform of $S_p(t, x_p)$. The start region of the unwrapping for the wrapped phase of $S_p(t, x_p)$ contained the maximum value point of $S(t)$. The time on the middle sampling point was regarded as $t = 0$ s. Figure 4(a) shows the unwrapped phase of $z_c(t)$.

Assuming that the PZT moves with a constant acceleration, the movement of the PZT is expressed by a quadratic function $z_R(t) = at^2 + bt + c$. The movement $z_R(t)$ of the PZT is obtained from second-order polynomial fitting of $z_c(t)$, as shown in Fig. 4(b). The value of b is the average velocity V_a of the PZT, and it is equal to 60.98 μm/s. The non-linear component $z_v(t)$ is equal to $at^2 + h$, where $a = 16.56$ μm/s^2. The value of h is decided from the condition that $z_v(t) = 0$ at the first sampling point. The depth h of $z_v(t)$ is 16.7 nm, as shown in Fig. 4(c). The random movement $z_n(t)$ obtained by subtracting the $z_R(t)$ from the $z_c(t)$ is shown in Fig. 4(d), where its

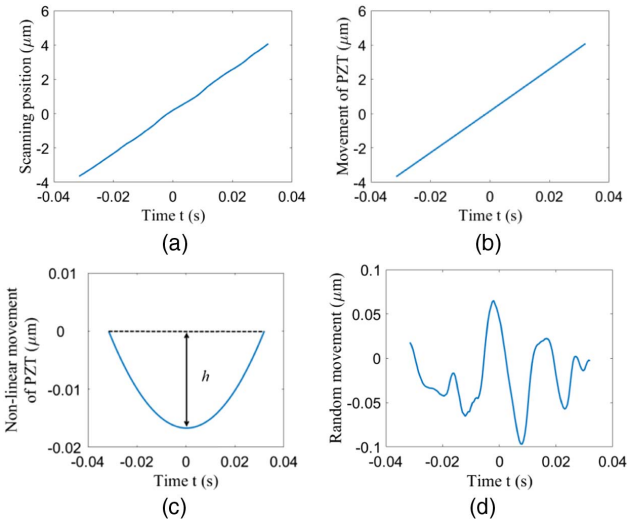

Fig. 4. (a) Scanning position $z_c(t)$ obtained from $S_p(t)$. (b) Movement $z_R(t)$ of the PZT obtained by second-order polynomial fitting. (c) Non-linear movement $z_v(t)$ of the PZT with $h = 16.7$ nm. (d) Random movement $z_n(t)$ with $\sigma_n = 36.0$ nm.

standard deviation σ_n is 36.0 nm. In simulations, the distributions of $V_a t$, $z_v(t)$, and $z_n(t)$ with different values of h and σ_n are used to generate the interference signal.

4. SIMULATION

First, it is explained how the interference signals were generated. The different magnitude of dispersion phase along x direction expressed by Eq. (3) brings an inclination along x direction to the measurement value z_p as reported in Ref. [7]. Therefore, it is reasonable to ignore the dispersion phase in the simulation for discussing the effects of non-linear movement of PZT, random movement, and additive noise. The interference signal given by Eqs. (1) and (4) were generated without $\varphi_d(\sigma)$. Figure 5 shows the spectrum $I(\sigma)$ of the supercontinuum light source detected with a spectral analyzer. Figure 6 shows the additive noise $n_A(t)$ obtained from experimental data, whose mean value is zero and standard variation is 0.11. The data of $z_c(t)$ in Fig. 4(a) were used as $z(t)$ in Eqs. (1) and (4) to generate the interference signals $S(t)$ and $S_p(t)$, and the object position z_o was equal to zero. The interference signal $S(t)$ scanned by $z(t)$ is shown in Fig. 7, where the additive noise $n_A(t)$ of Fig. 6 is contained with signal-to-noise ratio (SNR) = 10.1. It is a general method that the horizontal

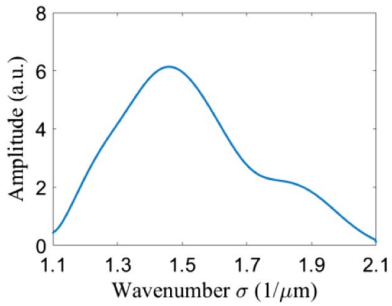

Fig. 5. Spectrum $I(\sigma)$ of the light source.

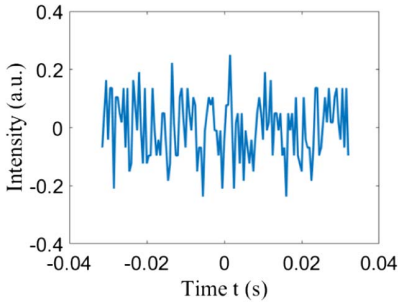

Fig. 6. Additive noise $n_A(t)$.

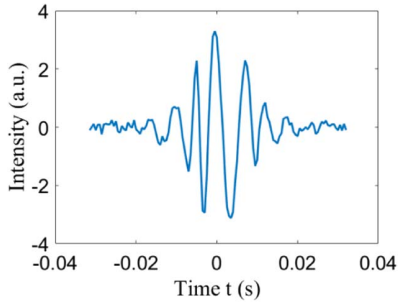

Fig. 7. Interference signal $S(t)$ scanned by $z(t)$.

axis t of $S(t)$ is regarded to have a relation of $z(t) = V_a t$ under the assumption that the PZT moves with a constant speed V_a. This interference signal is denoted by $S(z)$, where $z = 60.98t\,\mu$m. In our method the detected interference signal $S(t)$ in Fig. 7 was corrected by using the scanning position $z_c(t)$ and cubic spline interpolation. This corrected interference signal $S(z_c)$ is shown in Fig. 8, where the period of the sinusoidal waveform becomes almost constant. It is shown below that the measurement error in the corrected interference signal is less than a few nanometers.

Second, it was investigated how much the non-linear movement $z_v(t)$ of the PZT causes the measurement error of $z_p - z_o$. In this case, the scanning position was $z(t) = V_a t + z_v(t)$ with different values of h, and the random movement $z_n(t)$ and the additive noise $n_A(t)$ were equal to zero. Table 1 shows the measurement errors in the detected signal $S(z)$ and the corrected signal $S(z_c)$, respectively. The measurement error in $S(z)$ changes linearly with the increase in h. On the other hand,

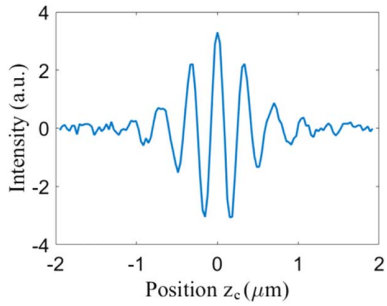

Fig. 8. Interference signal corrected by the scanning position $z_c(t)$.

Table 1. Measurement Errors Caused by $z_v(t)$ in $S(z)$ and $S(z_c)$

h (nm)	10	20	30
Error in $S(z)$ (nm)	10.1	20.2	30.3
Error in $S(z_c)$ (nm)	0.04	0.03	0.04

magnitude of the error in $S(z_c)$ is always less than 0.04 nm, regardless of the values of h. Therefore, it was clear that the correction of the interference signal by $z_c(t)$ could eliminate completely the measurement error caused by the non-linear movement of the PZT.

Third, in order to investigate effects of random movement $z_n(t)$, the scanning position was $z(t) = V_a t + z_v(t) + z_n(t)$ with $h = 20$ nm because of $h = 16.7$ nm in the experimental data. The additive noise $n_A(t)$ was equal to zero. A mean value (MV) and a standard deviation (SD) of the measurement error caused by random movement were calculated by using six different samples of noise $z_n(t)$ with the same standard deviation σ_n. Table 2 shows the measurement errors with different values of SD σ_n in $S(z)$ and $S(z_c)$. The MV of the error in $S(z)$ was dozens of nanometers and became larger with the increase in SD σ_n. The MV of the error in $S(z_c)$ was in the range of 0.03 nm to 0.54 nm, and the SD was almost equal to the MV. It was clear that the measurement error caused by $z_n(t)$ could be eliminated in $S(z_c)$, and the MV of the error was less than 0.5 nm in the region less than $\sigma_n = 60$ nm.

Finally, the interference signal $S(t)$ contained the additive noise $n_A(t)$, and the scanning position was $z(t) = V_a t + z_v(t) + z_n(t)$ with $h = 20$ nm and $\sigma_n = 40$ nm. SNR of the interference signal was defined as the ratio between the SDs of $S(t)$ and $n_A(t)$. The calculated measurement errors at different values of SNR are shown in Table 3. The MVs in $S(z_c)$ in Table 3 are very much larger than those at $\sigma_n = 40$ nm in Table 2.

The measurement error by non-linear movement of the PZT is very small compared with the errors caused by $z_n(t)$ and $n_A(t)$. Therefore, non-linear movement of the PZT does not have any effect on the measurement error in $S(z_c)$. The measurement errors by $z_n(t)$ are much smaller than those by $n_A(t)$ in $S(z_c)$, and the measurement error caused mainly by $n_A(t)$ is less than 2 nm in the actual experimental conditions.

Table 2. Measurement Errors Caused by $z_n(t)$ at $h = 20$ nm in $S(t)$ and $S(z_c)$

σ_n (nm)	20	40	60
MV of error in $S(z)$ (nm)	21.4	32.8	49.9
MV of error in $S(z_c)$ (nm)	0.03	0.18	0.54
SD of error in $S(z_c)$ (nm)	0.03	0.14	0.51

Table 3. Measurement Errors Caused by $n_A(t)$ at $h = 20$ nm and $\sigma_n = 40$ nm in $S(t)$ and $S(z_c)$

SNR	20	10	5
MV of error in $S(z)$ (nm)	32.0	32.4	33.8
MV of error in $S(z_c)$ (nm)	0.63	1.17	2.28
SD of error in $S(z_c)$ (nm)	0.40	0.70	1.36

5. EXPERIMENT

The WLSI shown in Fig. 1 was constructed. The object was a glass plate having two surfaces with a step of 3-μm height, and the two surfaces were denoted by A and B as shown in Fig. 1. The reference surface was a glass plate with a wedge angle, and the glass plate was regarded as one reflecting surface. The average speed of the reference mirror was 61 μm/s. Pixel size of the high-speed camera was 20 × 20 μm, and its frame size was 640 × 480 pixels. In order to make the measurement points with intervals of 200 μm, an interference signal detected on one pixel was selected every 10 pixels along x and y directions. The measuring points of $S(t, x, y)$ were denoted by N_x and N_y, where N_x was from 1 to 51, and where N_y was from 1 to 41. Central wavelength and bandwidth of the band-pass filter were 633 nm and 3 nm, respectively. The interference signal $S_p(t)$ detected with the photodiode was transferred to a computer with an A-D converter. A start trigger and an external sampling clock of 2 KHz were provided to the high-speed camera and the A-D converter to capture the interference signals. The number of the sampling points of the $S_p(t)$ and $S(t)$ was 1024. Figure 9(a) shows the interference signal $S_p(t)$ whose average period and full width at half maximum are about 5 ms and 65 μm, respectively. Figure 9(b) shows the sum of non-linear movement $z_v(t)$ and random movement $z_n(t)$ contained in the scanning position $z_c(t)$ obtained from $S_p(t)$. Figure 10(a) shows the interference signal $S(t)$ detected on a measurement point of $N_x = 10$ and $N_y = 20$ at the surface A. The interference signal $S(z_c)$ corrected by the scanning position $z_c(t)$ is shown in Fig. 10(b). It is shown clearly that the corrected signal $S(z_c)$ consists of a sinusoidal wave form with an almost constant period compared to the signal $S(t)$.

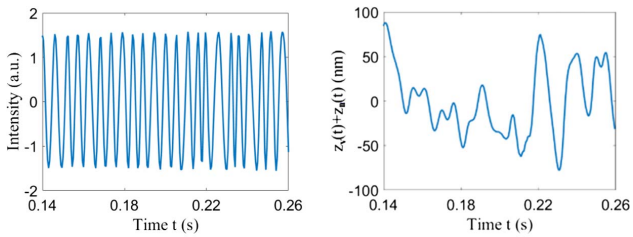

Fig. 9. (a) Interference signal $S_p(t)$ detected with the photodiode. (b) Sum of the non-linear movement $z_v(t)$ and random movement $z_n(t)$ contained in the scanning position $z_c(t)$ obtained from the $S_p(t)$.

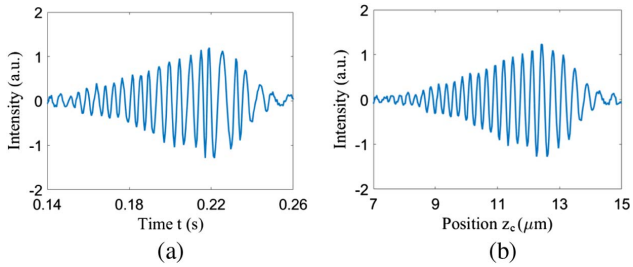

Fig. 10. (a) Interference signal $S(t)$ detected at a measurement point of $Nx = 10$ and $Ny = 20$. (b) Corrected interference signal $S(z_c)$.

The signal processing to obtain the measurement value z_p was carried out for all of the measurement points to get surface profiles of the object. The measurements were repeated three times at intervals of about 10 min. These measurements were called as M1, M2, and M3. The surface profile obtained from the signal $S(t)$ or $S(z)$ in M1 are shown in Figs. 11(a) and 11(b), where the tilt and piston components are eliminated. In order to show clearly the small variations, surface A and B are shown separately. The step height between the two surfaces was 2.839 μm, as shown in Fig. 12. Figure 13 shows one-dimensional surface profiles at $Nx = 10$ obtained from $S(z)$ in the three measurements. SD σ_n of $z_n(t)$ were 30.9 nm in M1, 7.6 nm in M2, and 21.5 nm in M3. The repeatability of the profiles on surface A and surface B were 6.0 nm and 6.2 nm, respectively. The magnitude of the small variations on the two surfaces was less than 30 nm.

Next, the corrected signal $S(z_c)$ was used for the three measurements of M1 to M3. The profiles of surface A and surface B obtained from the $S(z_c)$ in M1 are shown in Figs. 14(a) and 14(b), respectively. The measured step height was 2.963 μm, as shown in Fig. 15. This measured value was consistent with the nominal values of 2.95–3.05 μm caused by an error of the manufacture. Figure 16 shows one-dimensional surface profiles at $Nx = 10$ obtained from $S(z_c)$ in the three measurements. Compared with the distributions in Fig. 13, the three

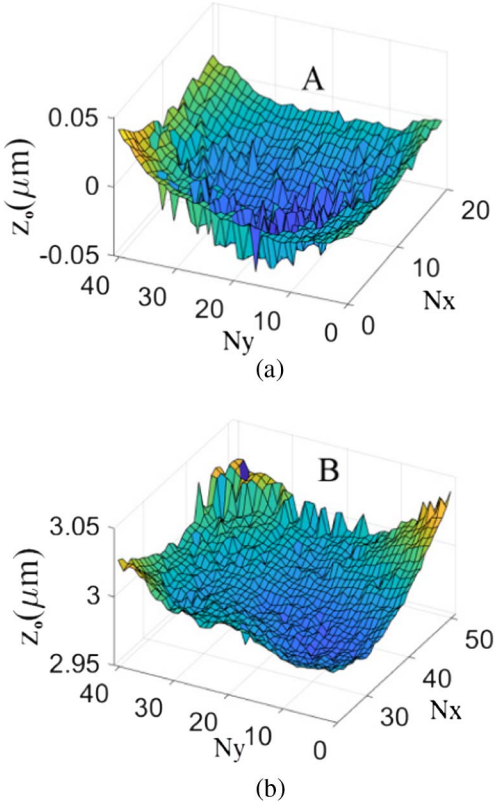

Fig. 11. Profiles of (a) surface A and (b) surface B obtained from $S(z)$.

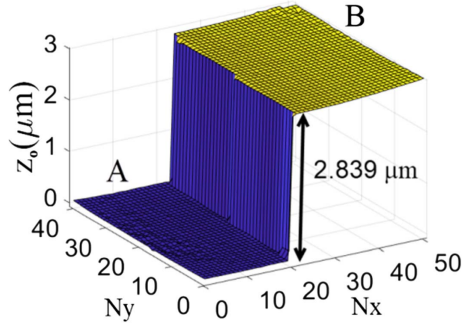

Fig. 12. Surface profile obtained from $S(z)$.

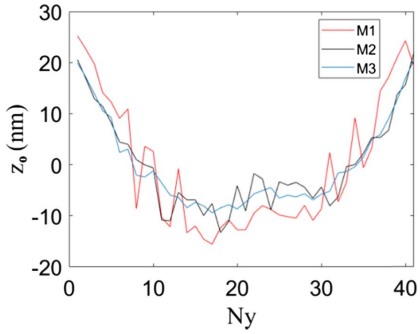

Fig. 13. One-dimensional surface profiles at $Nx = 10$ obtained from $S(z)$ in the three measurements.

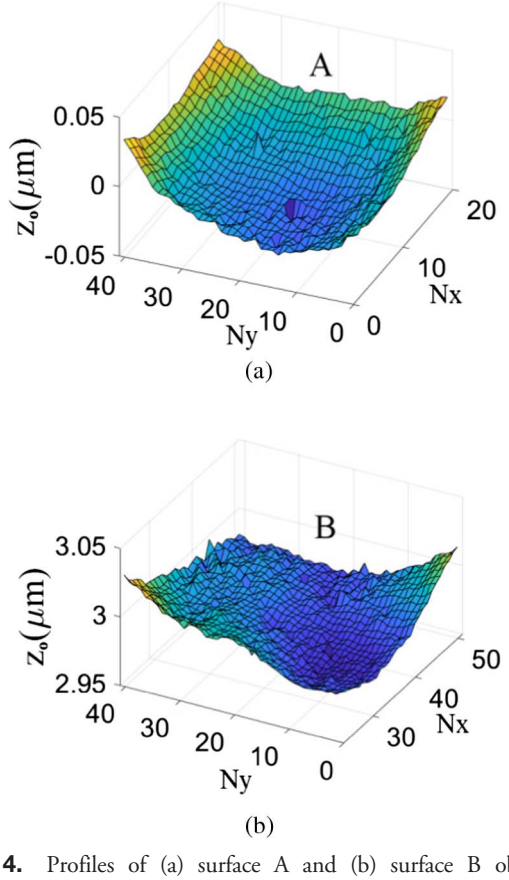

Fig. 14. Profiles of (a) surface A and (b) surface B obtained from $S(z_c)$.

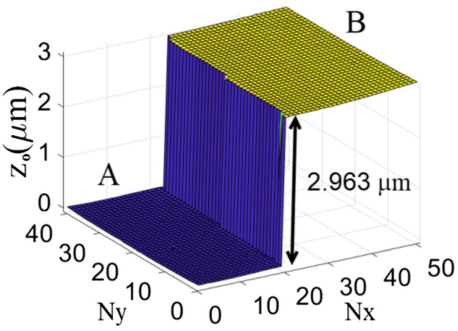

Fig. 15. Surface profile obtained from $S(z_c)$.

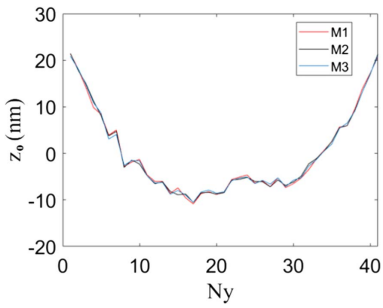

Fig. 16. One-dimensional surface profiles at $Nx = 10$ obtained from $S(z_c)$ in the three measurements.

measurement results in Fig. 16 are almost the same, and the measurement repeatability of surface A and surface B is 0.5 nm and 0.6 nm, respectively. The magnitude of the small variations on the two surfaces was less than 2 nm. It was clear that the interference signal corrected by the scanning position $z_c(t)$ provided a more exact measurement value z_b for the surface profiles.

6. CONCLUSION

The additional interferometer was simply equipped in the WLSI by using the light source of the WLSI, the beam splitter, the optical band-pass filter, and the photodiode without negatively influencing the WLSI. The actual OPD was easily calculated from the interference signal detected with the photodiode through the same signal processing as that in the WLSI. The scanning positions of the interference signal in the WLSI were corrected by the actual OPD values, and the corrected interference signal with a constant sampling interval was obtained by cubic spline interpolation. It was shown that the actual OPD or the scanning position changing with time contained the linear and non-linear movement of the PZT and random movement by external disturbances. It was clear in simulations that non-linear movement did not cause any measurement error, and random movement caused a small measurement error less than about 0.5 nm in the corrected interference signal. The additive noise contained in the interference signal of the WLSI caused a measurement error of a few nanometers in the simulations, which means that the additive noise is a main source of the measurement error after eliminating the measurement errors by non-linear movement and random movement. With the correction method, a surface profile with a step shape of 3-μm height was measured accurately with an error less than 2 nm.

Funding. National Natural Science Foundation of China (NSFC) (61575070).

Acknowledgment. The experiments of this research were carried out in Huaqiao University.

REFERENCES

1. A. Harasaki, J. Schmit, and J. C. Wyant, "Improved vertical-scanning interferometry," Appl. Opt. **39**, 2107–2115 (2000).
2. R. Hahn, J. Krauter, K. Körner, M. Gronle, and W. Osten, "Single-shot low coherence pointwise measuring interferometer with potential for in-line inspection," Meas. Sci. Technol. **28**, 025009 (2017).
3. P. de Groot and L. Deck, "Surface profiling by analysis of white-light interferograms in the spatial frequency domain," J. Mod. Opt. **42**, 389–401 (1995).
4. M. B. Sinclair, M. P. de Boer, and A. D. Corwin, "Long-working-distance incoherent-light interference microscope," Appl. Opt. **44**, 7714–7721 (2005).
5. P. de Groot, X. C. de Lega, J. Kramer, and M. Turzhitsky, "Determination of fringe order in white-light interference microscopy," Appl. Opt. **41**, 4571–4578 (2002).
6. S. Luo, O. Sasaki, Z. Chen, and J. Pu, "Utilization of complex-valued signals in a white-light scanning interferometer for accurate measurement of a surface profile," Appl. Opt. **56**, 4419–4425 (2017).
7. S. Luo, O. Sasaki, Z. Chen, S. Choi, and J. Pu, "Exact surface profile measurement without subtracting dispersion phase through Fourier transform in a white-light scanning interferometer," Appl. Opt. **57**, 894–899 (2018).
8. S. Kiyono, W. Gao, S. Zhang, and T. Aramaki, "Self-calibration of a scanning white light interference microscope," Opt. Eng. **39**, 2720–2725 (2000).
9. S. Kim, M. Kang, and S. Lee, "White light phase-shifting interferometry with self-compensation of PZT scanning errors," Proc. SPIE **3740**, 16–19 (1999).
10. J. Schmit and A. Olszak, "High-precision shape measurement by white-light interferometry with real-time scanner error correction," Appl. Opt. **41**, 5943–5950 (2002).
11. J. Liesener, M. Davidson, P. de Groot, X. C. de Lega, and L. Deck, "Low coherence interferometry with scan error correction," US patent 8, 902, 431 B2 (December2, 2014).
12. D. Chen, J. Schmit, and M. Novak, "Real-time scanner error correction in white light interferometry," Proc. SPIE **9276**, 927601 (2014).
13. A. Olszak and J. Schmit, "High-stability white-light interferometry with reference signal for real-time correction of scanning errors," Opt. Eng. **42**, 54–59 (2003).
14. S. Tereschenko, P. Lehmann, L. Zellmer, and A. Brueckner-Foit, "Passive vibration compensation in scanning white-light interferometry," Appl. Opt. **55**, 6172–6182 (2016).